ISTITUTO NAZIONALE DI FISICA NUCLEARE

Sezione di Padova

INFN/AE-88/3
18 Marzo 1988

N. Bacchetta, D. Bisello, A. Castro and J. Wyss:

A CHERENKOV RING IMAGING DEVICE FOR PARTICLE IDENTIFICATION IN A $B\bar{B}$ FACTORY DETECTOR.

A CHERENKOV RING IMAGING DEVICE

FOR PARTICLE IDENTIFICATION IN A $B\bar{B}$ FACTORY DETECTOR

INFN/AE-88/3
18 Marzo 1988

N. Bacchetta, D. Bisello, A. Castro and J. Wyss

Dipartimento di Fisica dell' Universita' di Padova
INFN, Sezione di Padova
I – 35131 Padua, Italy

Paper presented at the Workshop on Heavy Quarks Factory and Nuclear Physics Facility with Superconducting Linacs, Courmayeur, Italy, December 14-18 1987

1. – INTRODUCTION

During the past years a great interest has emerged for bottom physics. In particular the origin of the CP violation might be identified if intense sources of B mesons were available.[1] However bottom physics is characterized by a small efficiency in full event reconstruction. To enhance this capability unambiguous particle identification and very low gamma energy measurement must be assured over the whole solid angle. The interesting features of $B\bar{B}$ events are summarized in Tab. 1.

The necessary advances in accelerator and detector technologies are objects of studies in many European countries and in the USA.

In the following a particle identification device based on the Cherenkov Ring Imaging technique is presented. The device parameters are obtimized for ELISA[2] project, the proposed italian $B\bar{B}$ factory.

Since particle identification occurs before electromagnetic calorimetry the device must account for less than 20% radiation length, in order to permit good efficiency and energy resolution for photons.

Up to now available techniques for particle identification include:

- TOF's;
- dE/dx;
- Cherenkov ring imaging.

In the second generation detectors for $B\bar{B}$ physics, ARGUS and CLEO II, particle identification is done by combined TOF and dE/dx measurements: their performances[3] are summarized in Tab.2. The particle separation is shown in Fig.1 for ARGUS: an unambigous signature is achieved only up to 1 GeV/c, i.e. for half of the particles if the B are produced at threshold: this percentage dramatically drops in the continuum.

A better separation requires a TOF resolution below 100 psec, which could be obtained with Pestov counters. However the reliability of these devices for large surfaces has not yet been tested; in any case it seems difficult to limit their radiation length within the required value.

In the Cherenkov ring imaging technique the Cherenkov angle, which is proportional to the particle velocity, is directly measured. This technique, proposed by Seguinot and Ypsilantis[4] has been extensively studied and is at present used in large detectors at LEP, SLC and elsewhere. Full particle identification in the momentum range interesting for $B\bar{B}$ physics is achieved using the light emitted by liquid radiators. This solution, adopted by DELPHI[5] and SLD[6] foresees:

- C_6F_{14} liquid radiator with n=1.275 very close to the optimum n=1.2 value;
- photon conversion by TMAE at temperature $\simeq 30^0$C in a $CH_4 + C_2H_6$ mixture;
- long electron drift ($\geq$ 1 m) in an electric field parallel to the beams;
- electron detection by MWPC.

The photon conversion coordinates are given, x by the wire address, z by the drift time and y by charge division on the wire (SLD) or by cathodes ortogonal to the wires (DELPHI). Expected performances of such a detector are presented in Fig.2.

These detectors have to deal with many technical challenges. TMAE even at room temperature is very aggressive; furthermore it requires a large volume because a depth of about 5 cm is necessary to obtain full (97%) photon conversion. This thickness is also

necessary to produce long drift paths. The long drift technique demands a high electric field ($E \simeq 500$ V/cm) and consequently one must manage very high voltages ($V \simeq 50 \div 80$ kV). Furthermore efficient electron collection requires careful removal of impurities, and space and surface charges are a threat to precision in ring reconstruction. Feedback photons are produced in the multiplication region around the wires: they can convert in the drift region producing spurious signals and around the wires themselves causing a smearing of the resolution along the wire. The number of these photons can be reduced by lowering the amplification gain, but a higher gain is required if a cathode read-out is adopted. Finally long drift times can be used only in the presence of low interaction rates.

With high interaction rate machines the drift box with a small detector at the end has to be replaced by a fast detector covering the whole surface of the photoionization volume. An interesting alternative[7] in this environment is to operate with a very short photon convertion path ($\lambda \simeq 1$ mm). This can be obtained using TMAE at higher temperatures (Fig.3): at 85^0C full photon conversion is assured by a 4 mm path. However at higher temperatures the TMAE is probably even more aggressive and the UV absorption of gas impurities is enhanced. Both choice of materials and impurities control become critical. Finally more electronic channels are required by covering the large photoconversion region.

Nevertheless all the problems related to the long drift and very high voltages are avoided. Conversion of feedback photons can occur only within a small region and is largely reduced because the wire spacing is much larger than the conversion path.

Finally by lowering the detector thickness the detector volume following particle identification is considerably reduced, as it scales as $3 \times \Delta r/r$ for constant solid angle coverage.

It has been recently proposed to use solid radiators as NaF (CaF_2)[7]. This material exhibits good transparency properties and could be avalaible on large surfaces. However its refraction index is high ($n \simeq 1.4$), thus photons can be lost by total reflection, and n varies consiberably as a function of the photon energy enhancing the chromatic error. The behaviour of the refraction index n for NaF and C_6F_{14} is shown in Fig.4a and Fig.4b respectively.

Nevertheless a solid radiator is easier to handle and permits one to eliminate the quartz windows covering the liquid radiator, thus lowering the number of spurious photons and reducing the overall radiation length of the detector. Furthermore NaF (CaF_2) transmits photon over a larger energy range than quartz allowing the substitution of TMAE with TEA (Fig.5), which may be somewhat less difficult to operate with.

2. – PROPOSED DETECTOR

The proposed particle identification detector (Fig.6) is based on the Cherenkov Ring technique with solid NaF radiator, TEA as photoionization medium and MWPC electron detection. Although the interaction rate of the collider, 10 KHz, could permit the long drift technique, the short drift along the radius of the detector has been preferred because of:

- fewer HV problems;
- smaller gas volume;
- more compact dimensions.

The choice of TEA as photoionization medium allows the detector to run at room temperature and thermal control and shields are no longer necessary.

The available volume for the detector is a cylindrical barrel ranging from $R_{min} = 0.66$ m to $R_{max} = 0.85$ m and from $z = -1.13$ m to $z = 1.13$ m. No end-cap detectors are foreseen in order to reduce the radiation length in front of the electromagnetic calorimeter at small angles where the end plates of the drift chamber contribute. The barrel radiators and detectors are divided into sectors covering 30^0 in azimuthal angle; the local azimuthal coordinate will be called x in the following. Each sector covers one half of the length along the z coordinate. A drawing of a sector cross-section is shown in Fig.7.

The incident particle encounters in succession a honeycomb mechanical structure and then the NaF radiator. The large helium filled region follows, separated from the detection volume by a NaF window.† This last region is filled with a CH_4, C_2H_6 mixture with saturated TEA vapour at room temperature. The measurement of the photoelectrons coordinates is assured by a MWPC with 33 μm diameter carbon wires[8] strung along the x coordinate and spaced by 3.81 mm. No measurement is foreseen for the conversion depth coordinate while the second coordinate is given by charge division on the wire. This choice will be discussed in the following section.

The total radiation length of such a configuration amounts to $\simeq$ 13.5% X_0 for a normally incident particle.

3. – MEASUREMENT RESOLUTION

In the charge division method the two coordinates are given by the wire address z and by the measurement of the charge integrated at both ends of the wire. The coordinate x along the wire is:

$$x = \Delta Q \times \frac{L}{2} \quad \text{with } \Delta Q = \frac{Q_R - Q_L}{Q_R + Q_L}$$

where L is the wire length. Note that the wire resistivity has to be much greater than the input impedance of the amplifier in order to maximize resolution in x. The x measurement error depends on the charge error as:

$$\frac{\sigma_x}{x} = \frac{\sigma_Q}{Q}$$

The charge error can be espressed by the Equivalent Noise Charge which is the essentially the sum of two terms, thermal noise and voltage amplifier noise. Two other terms, shot noise and 1/F noise can be neglected in the present case. Thus the Equivalent Noise Charge for a shaping circuit with one differentiation and one integration can be written as:

$$ENC^2 = (\frac{2.718}{Q})^2 \times (\frac{kT\tau}{2R} + \frac{kTR_{eq}C^2}{2\tau})$$

† Cherenkov emission in such a window produces only a small smearing of the radiating particle signal in the MWPC.

where Q is the electron charge (Coulombs), k the Boltzmann constant (J/^{0}K), T the absolute temperature, τ the time constant of the amplifier (sec), R the wire resistivity (Ω), R_{eq} the resistivity of equivalent noise at the JFET input (Ω), and C the total input capacity (pF). In the following the values τ= 40 nsec, R = 20 KΩ, R_{eq} = 50 Ω, and C = 25 pF have been used.

The second term gives an ENC of 680 electrons, which is pessimistic since the SLD group[9] reported a value of 500 e^-. The sum of the two terms gives around 1200 electrons of ENC. Using a more sophisticated electronics this value could be reduced by 20%.

With the amplification gain of 2×10^5, used by SLD, the position error along the wire is:

$$\frac{\sigma x}{x} = \frac{\sigma Q}{Q} = 0.6\%$$

wich corresponds to 2.4 mm on a 40 cm long wire. This value can be reduced by working at higher gains. Thus a 0.4% value has been assumed in the detector simulation.

An alternative read-out would be provided by dividing the cathode surface into pads. In this case the ENC can be espressed in electron charges squared as:

$$ENC^2 = 5.8 \times 10^8 \times \frac{\tau_0}{R_p} + 3.6 \times 10^4 \times e_n^2 \frac{C^2}{\tau_0}$$

where τ_0 is the time constant of the amplifier (nsec), R_p the equivalent input resistor (Ω), C the capacitance (pF) and e_n the spectral density of the equivalent input noise voltage (nV/$\sqrt{\text{Hz}}$). In the proposed configuration, C = 11.4 pF and R_p = 1 KΩ, so assuming e_n = 3 nV/$\sqrt{\text{Hz}}$, the calculated values are ENC $\simeq$ 3400 e^- and $\simeq$ 3700 e^- for τ_0 = 1 nsec and 5 nsec respectively.

Taking a Furry pulse distribution for the detector and preamplifier output:

$$P(g) = \frac{1}{g_{ave}} e^{-g/g_{ave}}$$

and integrating this expression from the threshold value $g_{th} = 6.5 \times 10^3$ e^-, set as two times the noise value, to infinity gives the total detection efficiency. For 95% detection efficiency $g_{ave} = 1.3 \times 10^5$. This value however has to be multiplied by a factor 4 because for τ_0 = 5 nsec only 25% of the avalanche is developed and by a further factor 2 because of the anode-cathode coupling efficiency. Thus the final gain value is $g_{ave} = 10^6$.

Although some parameters of this calculation may be subject to variations the required gain for operating with a pad read-out is substantially higher, which is a familiar result. Nevertheless such gains are entirely feasible and already achieved.

4. – DETECTOR SIMULATION

The Monte Carlo simulation has been performed with the set-up of Fig.7. Losses at radiator and detector joints have been neglected. The program generates Cherenkov

radiation from a particle of given momentum and direction incident into the NaF radiator. Photons are produced according to:

$$\frac{dN}{dE} = \frac{2\pi\alpha}{hc} \times (1 - \frac{1}{\beta^2 n^2(E)}) \times Q(E) \times l$$

where l is the path length in the radiator and Q(E) is the TEA quantum efficiency. The distribution in the azimuthal angle around the particle direction is assumed to be uniform. Each generated photon is followed through the various materials from the radiator to the MWPC detector, taking into account the reflection probability at the surfaces, and the absorption probability in the materials. Finally an overall electron counting efficiency, $\epsilon = 80\%$, has been assumed to account for detection inefficiency, dead areas and unexpected losses. The coordinates of the detected photoelectrons have been fit by a reconstruction program.

The resolution on position measurement by the MWPC has been assumed to be $\sigma_x = 1.6$ mm, from charge division on the wire, while the precision on z depends on the wire spacing, which in the initial Monte Carlo runs was taken to be 2.54 mm. No measurement on the photon conversion depth in TEA being performed, the y coordinate in the MWPC has been assumed to be the mean depth of the chamber. The resolutions on the primary particle direction have been set to $\sigma_\theta = 0.3/sin\theta$ and $\sigma_\phi = 0.4$ mrad [7] in the following.

The values used for the transmission T of the NaF (11 mm thick)[7] and the TEA quantum efficiency[10] corrected for the CH_4 absorption are reported in Fig.5 as a function of the photon energy. For the quantum efficiency, where different measurements[10,11] are in disagreement, the more pessimistic one has been assumed.

Simulations have been done for two choices of radiator thickness and lever arm, l = 10 mm, L = 15 cm, and l = 7 mm, L = 12 cm respectively.

Fig. 8 gives the number of detected photoelectron as a function of θ_p, angle between the particle direction and the normal to the radiator surface, for π's and protons of 2 GeV/c. The curves show the effect of the total internal reflection for pions at $\theta_p \simeq 0^0$.

Fig.9a and Fig.9b show for the two geometrical configurations the different contributions to the error $\Delta\theta_C$ on the reconstructed Cherenkov angle for a single photoelectron as a function of θ_p. The dominant contribution is the chromaticity, i.e. the smearing of the Cherenkov angle due to the dependence on the photon energy of the refraction index and the transmission of different materials. The geometric error, which looks very important at high θ_p, arises from the assumption made in the reconstruction program that the photon has been emitted in the middle of the radiator. The chromatic error is due to assuming an average value ($E_{ave} = 8.05$ eV) of the photon energy in the reconstruction program; this error becomes negligible increasing θ_p. The position error is the precision on the photoconversion point measurement. Finally the particle error, due to the errors on the direction measurement of the incident particle, is very small ($\simeq$ 1mrad) and has not been reported on the figures.

The total error, obtained by adding all sources in quadrature, is almost constant, $\Delta\theta_C = 12 \div 13$ mrad, over the full θ_p range.

Fig.10a and Fig.10b show particle separation as a function of θ_p at fixed momentum,

and as a function of p with a fixed incident angle $\theta_p = 30^0$ (Fig.11). The discrimination between two hypothesis for a given particle momentum and incidence angle is defined by:

$$N_\sigma = \frac{\theta^i_{ave} - \theta^j_{ave}}{\Delta\theta^i} \times \sqrt{N^i_{pe}}$$

where $\theta^{i,j}_{ave}$ are the mean value of the measured Cherenkov angle for particles i and j, $\Delta\theta^{i,j}$ is the measurement error of the Cherenkov angle and $N^{i,j}_{pe}$ is the number of detected photoelectrons.

A value of $N_\sigma = 4.2$ which corresponds to a 1% level of misidentification is obtained up to 0.8 GeV/c for e/π, 2.5 GeV/c for π/K and 4 GeV/c for K/p. These values do not vary as a function of θ_p, except for $\theta_p \leq 5^0$. In fact below this incidence angle the Cherenkov photons emitted are trapped by internal total reflection into the radiator; that happens for different values of particle momentum as shown in Fig.12. The estimate of the loss of efficiency from this effect requires a full $B\bar{B}$ simulation. This aspect is under study.

Finally the simulation has been performed assuming a MWPC wire spacing of 3.81 mm, thus reducing by 33% the number of electronics channels. The particle identification capability of the detector is mantained into the previous momentum range, and is lowered by a few percent for large θ_p values.

5. – CONCLUSIONS

A Cherenkov Ring Imaging device with a 0.7 cm solid NaF radiator gives good π, K, p separation in the operational momentum range. Below Cherenkov threshold particle identification is assured by dE/dx measurements in the central tracking device. The choice of wire read-out permits lower gains thus reducing the number of feedback photons. Carbon wires of 50 kΩ/m resistivity and 3.81 mm spacing assure the required performance. The total number of electronic channels is not very large thus reducing the cost and the electronics management.

Acknowledgements

We would like to thank Matteo Cavalli-Sforza who has assisted in this work with continuous indications and criticism and Jacques Seguinot for helpful and clarifying discussions and for providing us with some unpublished results.

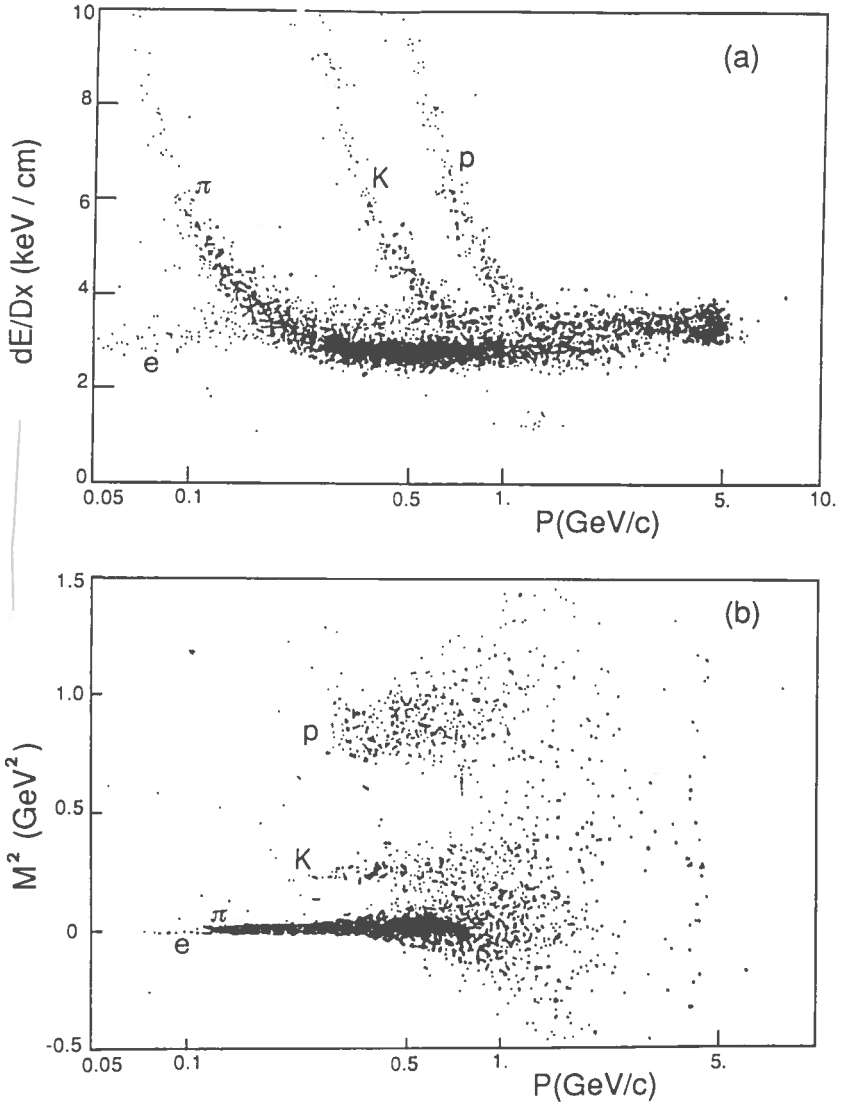

Fig.1 ARGUS particle identification from dE/dx (a) and TOF (b) measurements.

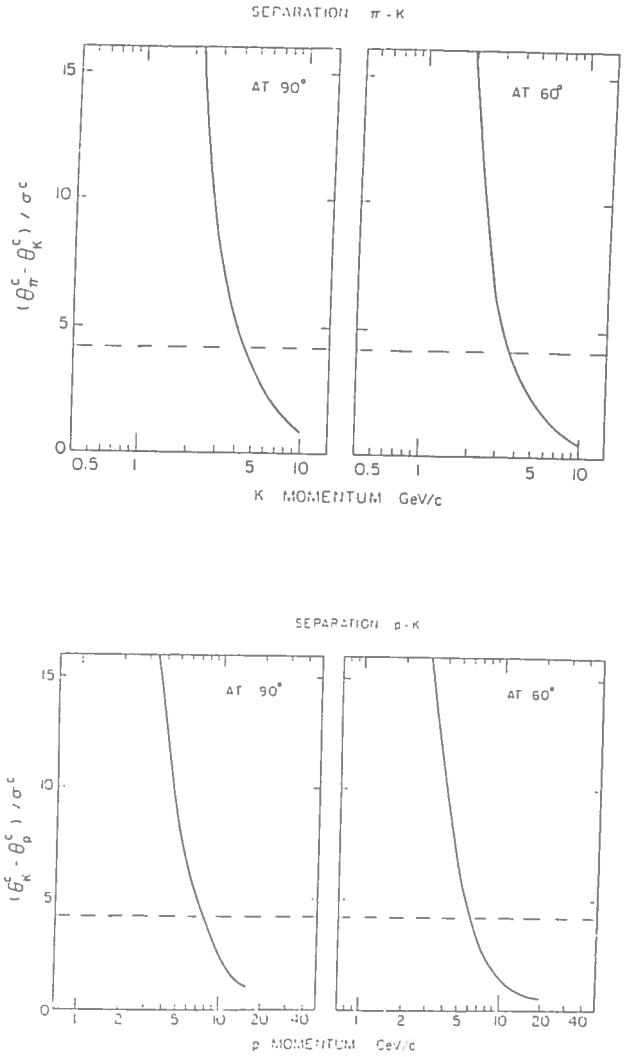

Fig.2 Estimated DELPHI π/K and K/p separation with liquid radiator.

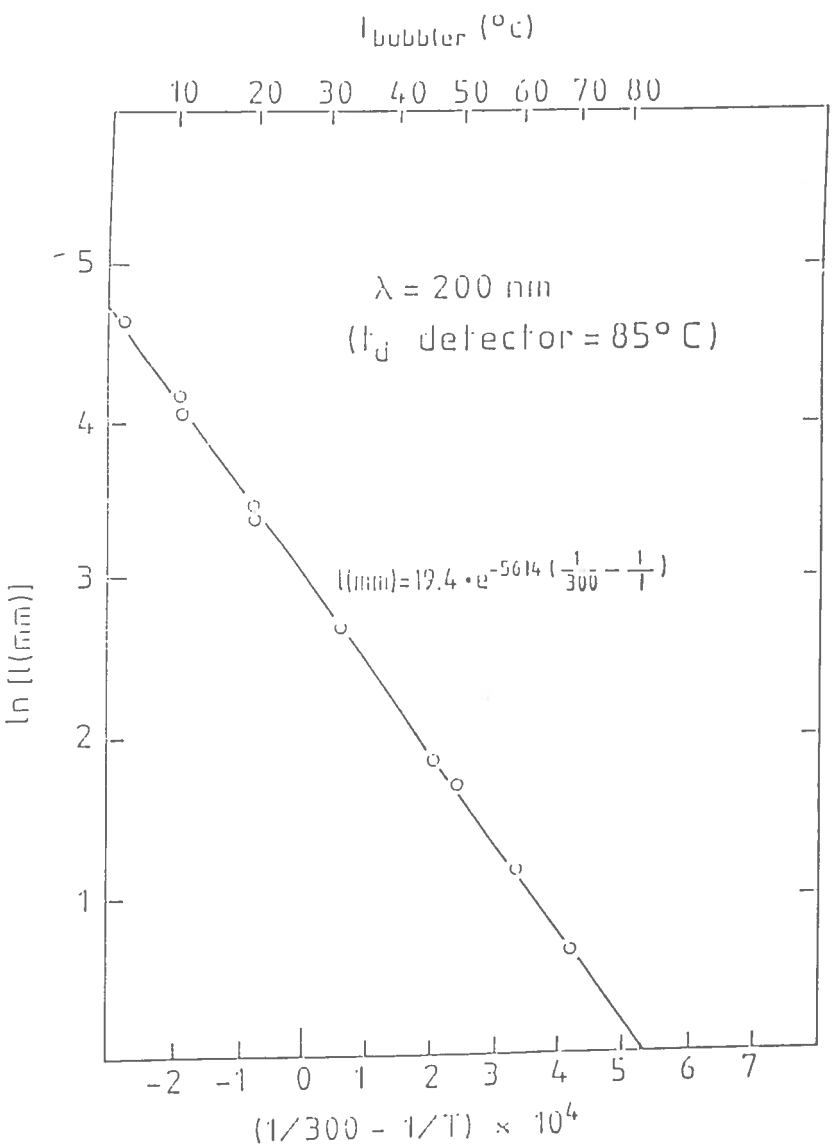

Fig.3 Photoconversion path in TMAE versus TMAE temperature (J.Seguinot private comunication).

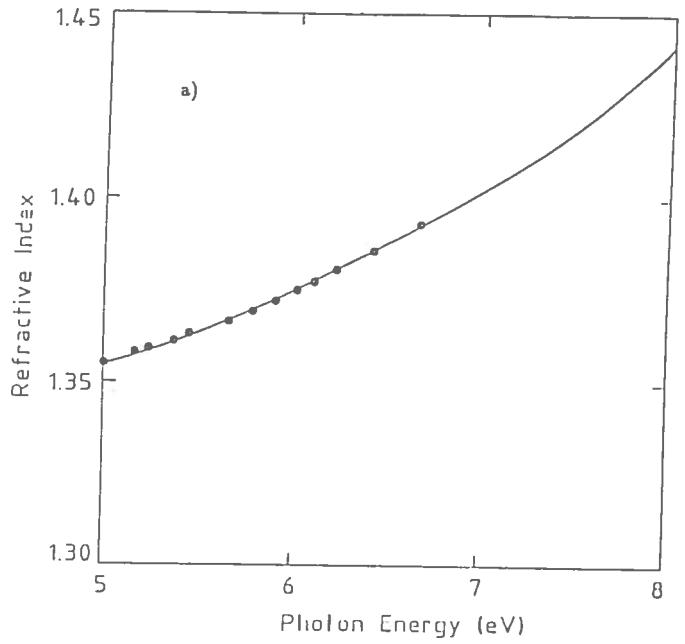

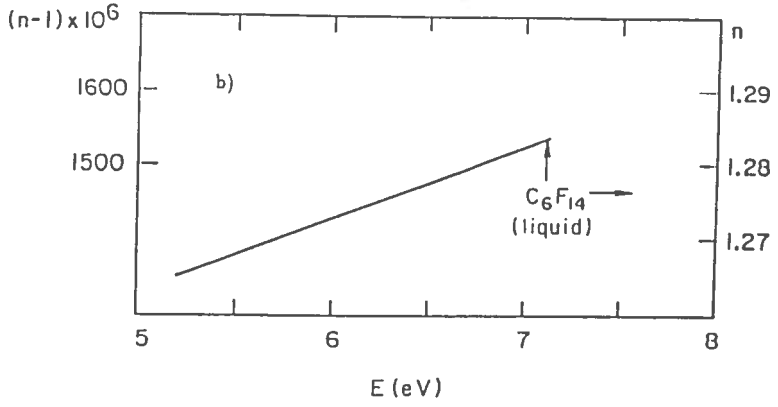

Fig.4 Refractive index n of NaF (from ref.[7]) and C_6F_{14} (from ref.[6]) versus the photon energy.

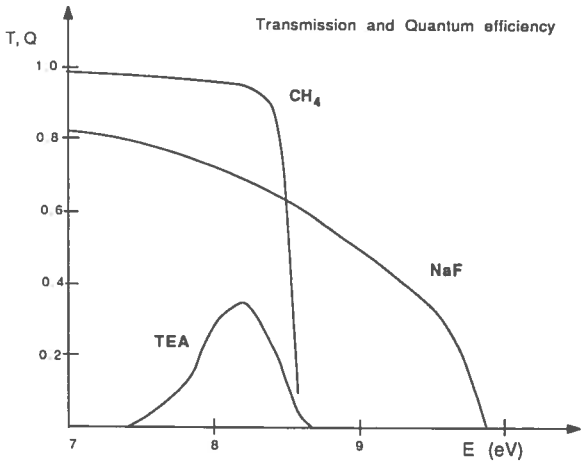

Fig.5 NaF trasmission (from ref.[7]) and TEA quantum efficiency with CH_4 cut-off (from ref.[11]) versus the photon energy.

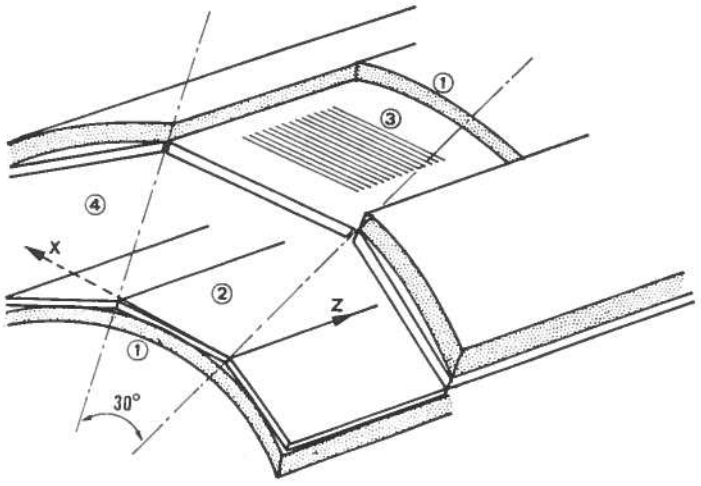

① Honeycomb vessel
② NaF radiator
③ Detector
④ He filled region

Fig.6 Schematic view of the detector.

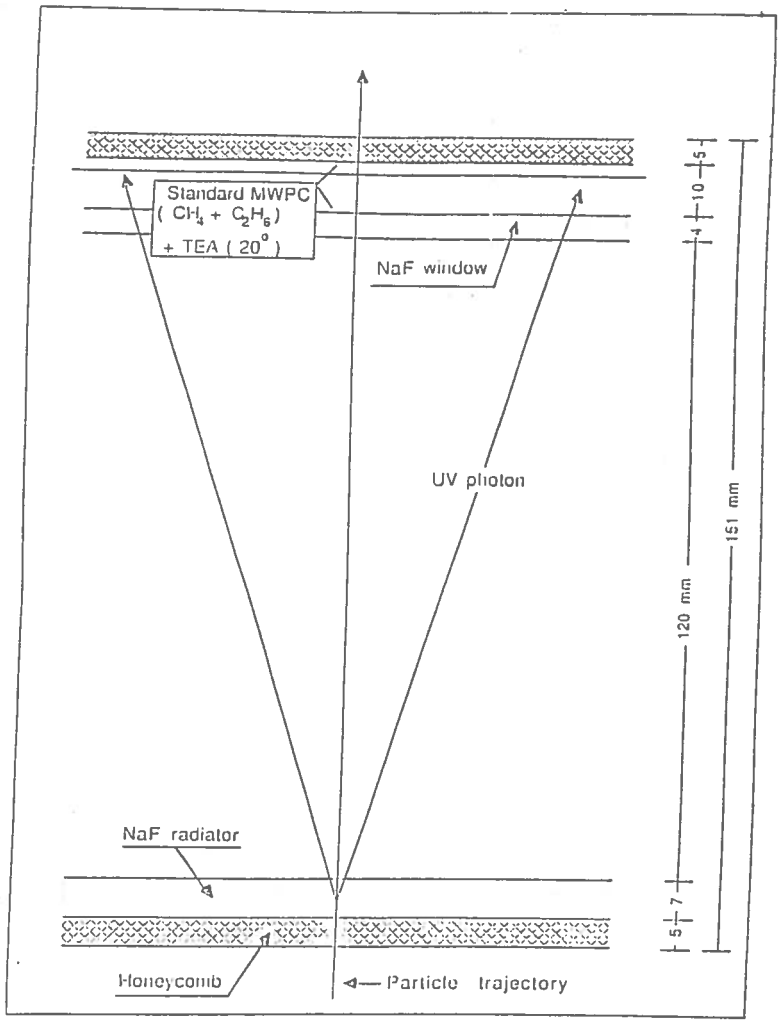

Fig.7 Sector cross section.

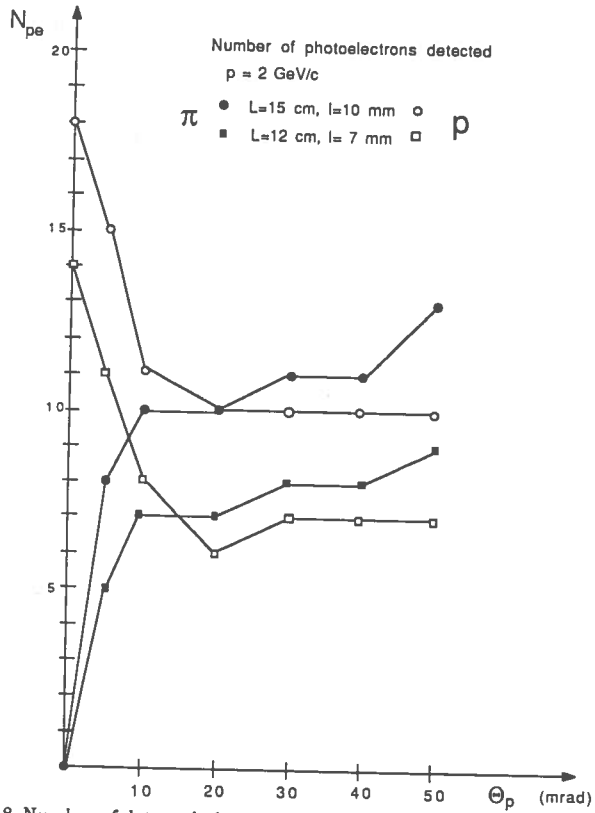

Fig.8 Number of detected photoelectrons versus the incidence angle of 2 GeV/c momentum π and p for L = 15 cm, l = 1 cm and L = 15 cm, l= 0.7 cm.

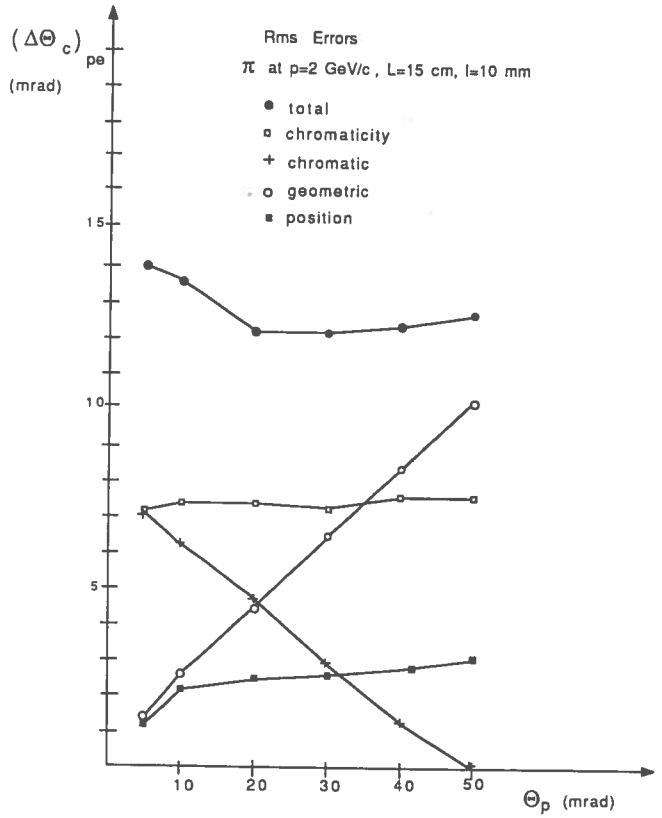

Fig.9 a Total $\Delta\theta_C$ for a 2 GeV/c momentum π versus the incidence angle with the contributions from cromaticity and chromatic, geometric and position error for L = 15 cm and l = 1 cm

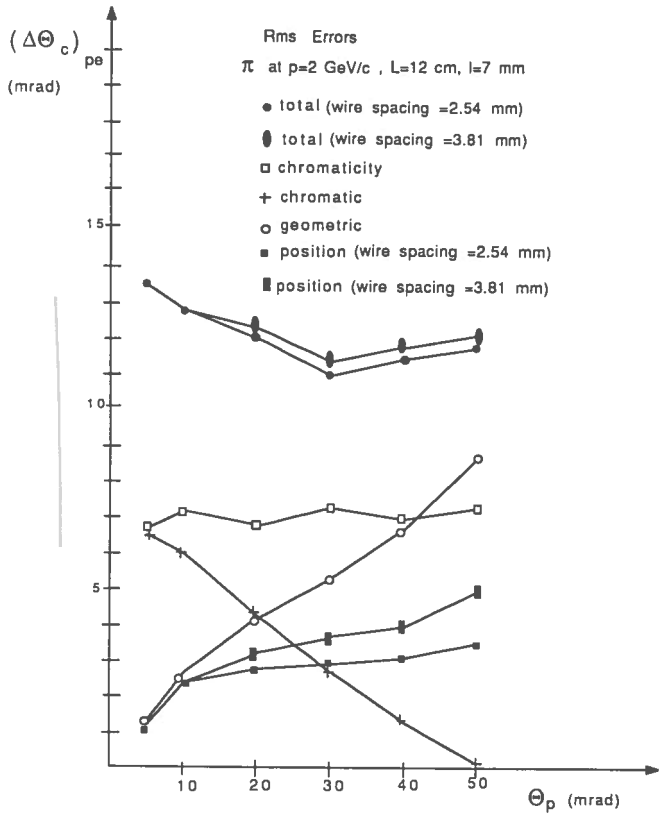

Fig.9 b Total $\Delta\theta_C$ for a 2 GeV/c momentum π versus the incidence angle with the contributions from cromaticity and chromatic, geometric and position error for L = 12 cm and l = 0.7 cm

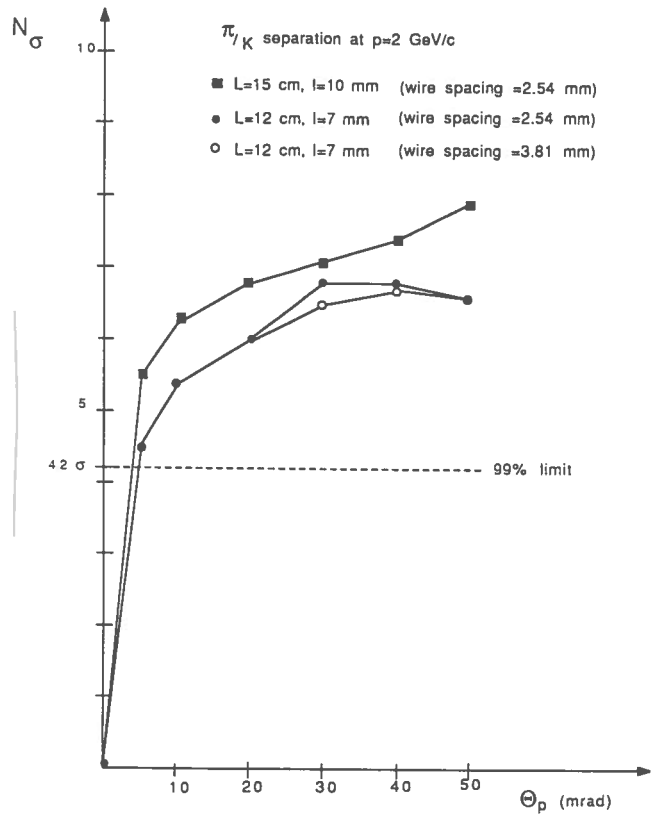

Fig.10 a π/K separation versus the incidence angle for a 2 GeV/c momentum particle for L = 15 cm, l = 1 cm and σ_z = 2.54 mm, L = 12 cm l = 0.7 cm and σ_z = 2.54 mm and for L = 12 cm, l = 0.7 cm and σ_z = 3.81 mm

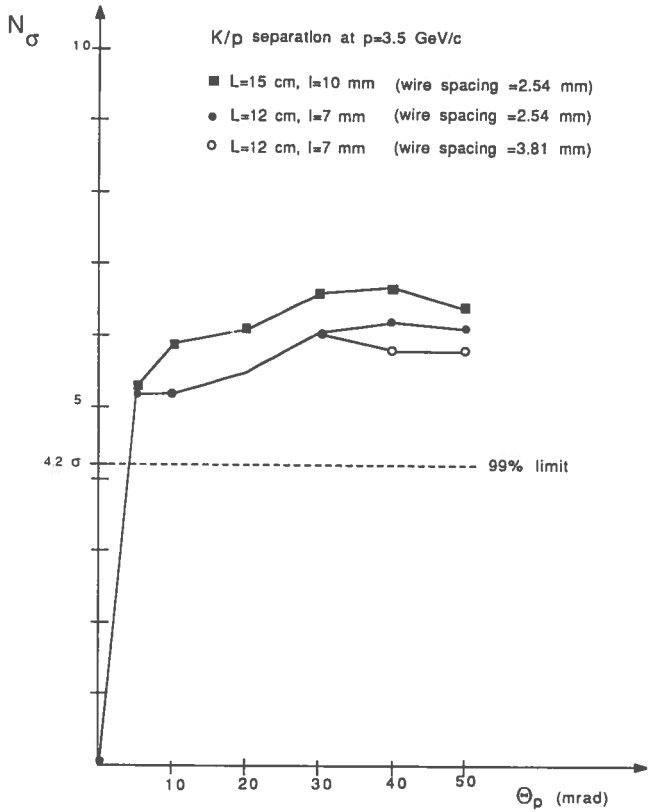

Fig.10 b K/p separation versus the incidence angle for a 2 GeV/c momentum particle for L = 15 cm, l = 1 cm and σ_z = 2.54 mm, L = 12 cm l = 0.7 cm and σ_z = 2.54 mm and for L = 12 cm, l = 0.7 cm and σ_z = 3.81 mm

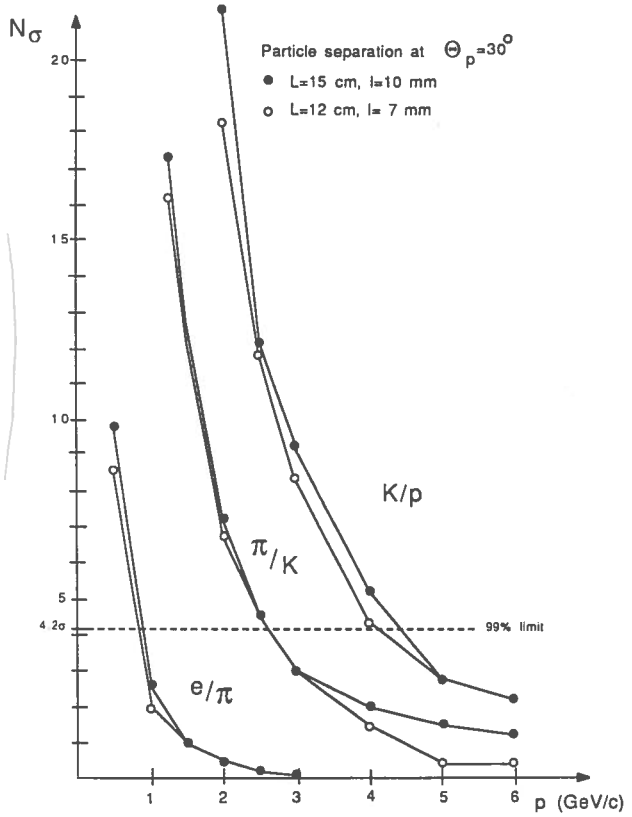

Fig.11 Particle separation at $\theta_p = 30^0$ versus the particle momentum in GeV/c, for L = 15 cm, l = 1 cm and L = 12 cm, l = 0.7 cm. Data refer to $\sigma_z = 2.54$ mm; no differencies are obtained for $\sigma_z = 3.81$ mm.

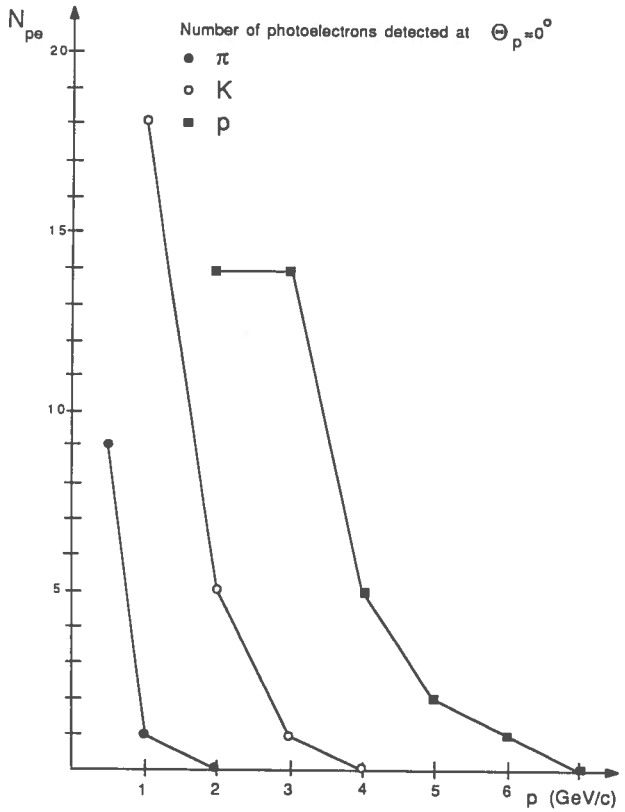

Fig.12 Number of photoelectrons detected at $\theta_p = 0^0$.

Table 1 Momentum mean values and mean multiplicities of $B\bar{B}$ events at the Y(4s).

$< E_\gamma >$	200 MeV/c^2
$< p_\pi >$	420 MeV/c
$< p_K >$	600 MeV/c
$< p_p >$	550 MeV/c
charged multiplicity	12
photon multiplicity	12

Table 2 Particle identification performances of ARGUS and CLEO II (from ref. [3]).

detector	CLEO II	ARGUS
resolution on dE/dx	6%	5%
resolution on TOF	200 *psec*	220 *psec*
3σ π/K separation up to	800 MeV/c	700 MeV/c
3σ K/p separation up to	1500 MeV/c	1200 MeV/c

References

1. For a recent theoretical overview see the Proceedings of the UCLA Workshop on Linear-collider $B\bar{B}$ Factory Conceptual Design, January 26-30 1987.
2. Proceedings of the Discussion Meeting on Physics Possibilities of a High Luminosity e^+e^- Facility up to $\sim$12 GeV, Frascati, Italy, April 22-23 1987.
   Proceedings of the Workshop on Heavy Quarks Factory and Nuclear Physics Facility with Superconducting Linacs, Courmayeur, Italy, December 14-18 1987.
3. E.Lorentz, Paper presented at the Topical Seminar on Heavy Flavours, San Miniato, Italy, May 25-29, 1987 (to be published in Supp. to Nuclear Physics B).
4. J.Seguinot and T.Ypsilantis, NIM 142 (1977), 377
5. R.Arnold et al., A Ring Imaging Cherenkov Detector. The DELPHI Barrel RICH Prototype. CRN/HE 87-01, 87-08
6. SLD Design Report, SLAC-27, UC-34D (1984)
7. R.Arnold et al., Paper presented at the London Conference on Position-Sensitive Detectors, London, September 7-11 1987, CERN-EP/87-186
8. J.Va'vra et al., Paper presented at the Nuclear Science Symposium, San Francisco, USA, October 21-23 1987; SLAC-PUB-4432 (1987)
9. E.Spencer et al., Paper presented at the Nuclear Science Symposium, San Francisco, USA, October 21-23 1987; SLAC-PUB-4404 (1987)
10. R.H.Holroyd et al., NIM A261 (1987), 440
11. T.Ekelof et al., Phys. Scr. 23 (1981), 718

A CHERENKOV RING IMAGING DEVICE

FOR PARTICLE IDENTIFICATION IN A $B\bar{B}$ FACTORY DETECTOR

N. Bacchetta, D. Bisello, A. Castro and J. Wyss

Dipartimento di Fisica dell'Universita' di Padova
INFN, Sezione di Padova
I – 35131 Padua, Italy

Paper presented at the Workshop on Heavy Quarks Factory and Nuclear Physics Facility with Superconducting Linacs, Courmayeur, Italy, December 14-18 1987

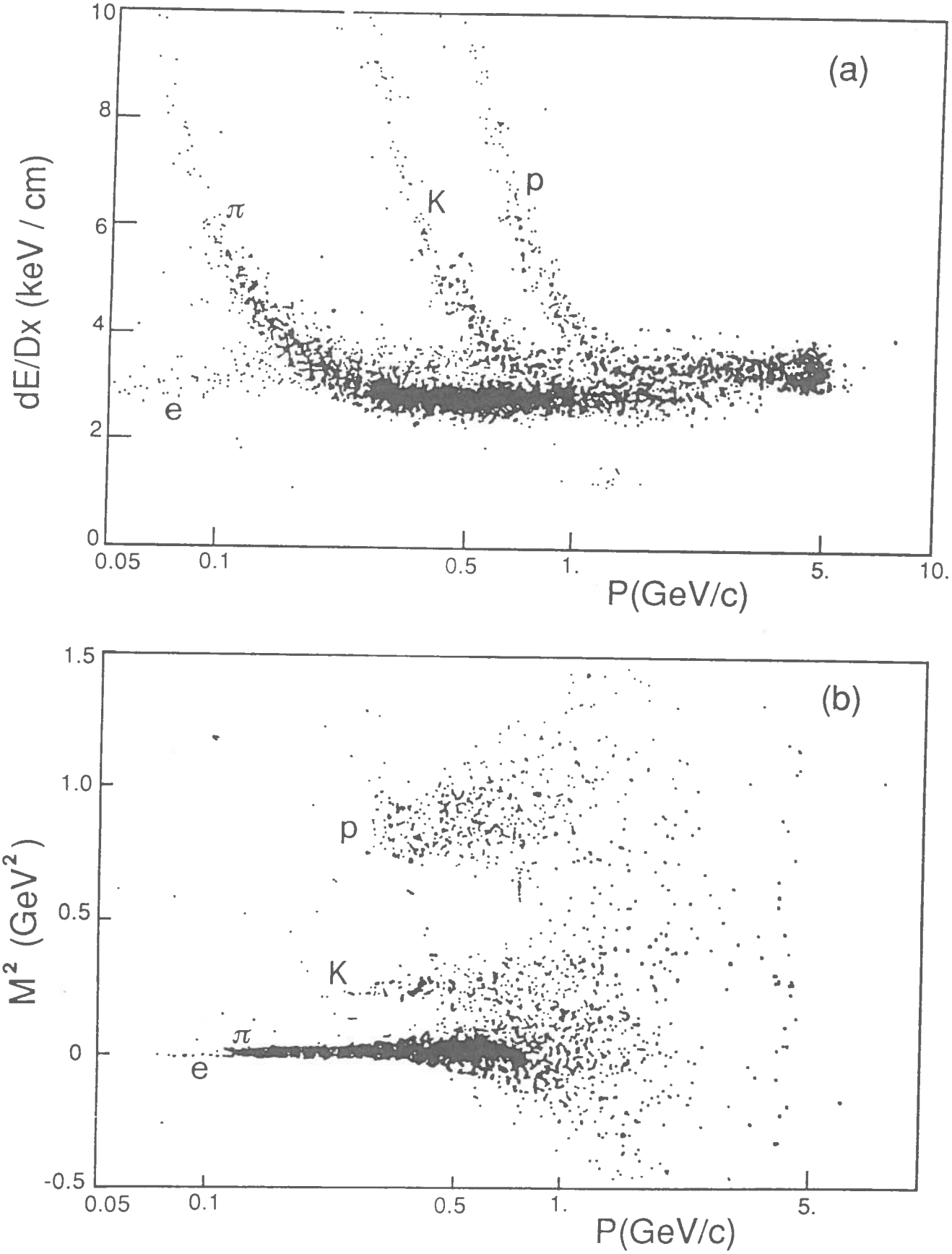

Fig.1 ARGUS particle identification from dE/dx (a) and TOF (b) measurements.

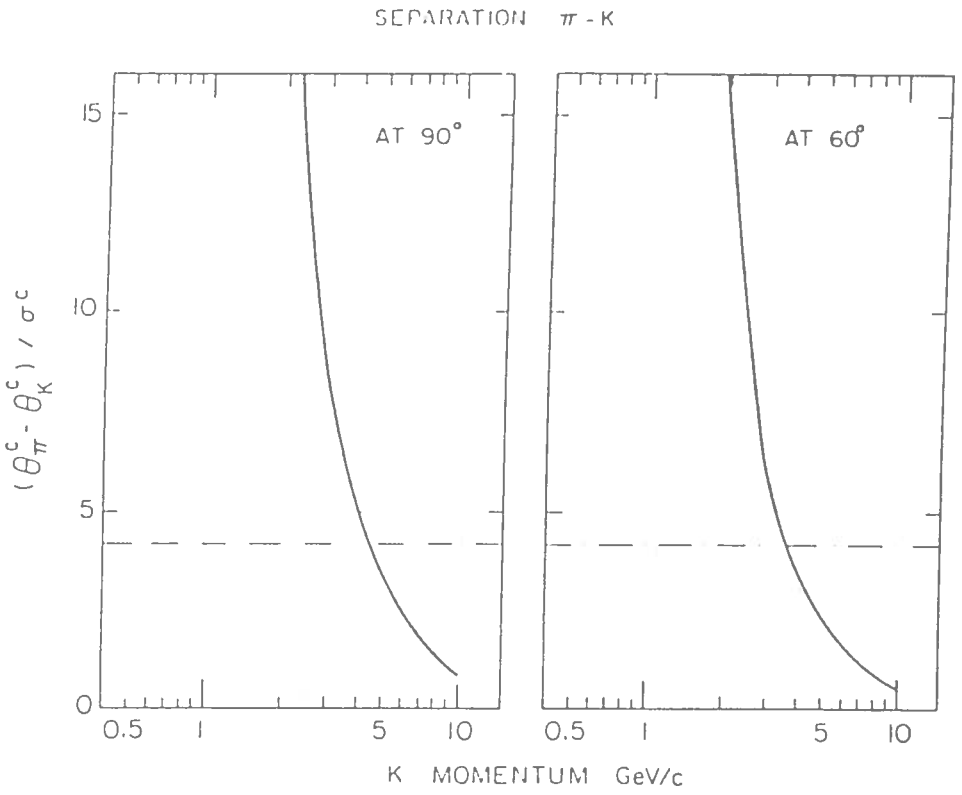

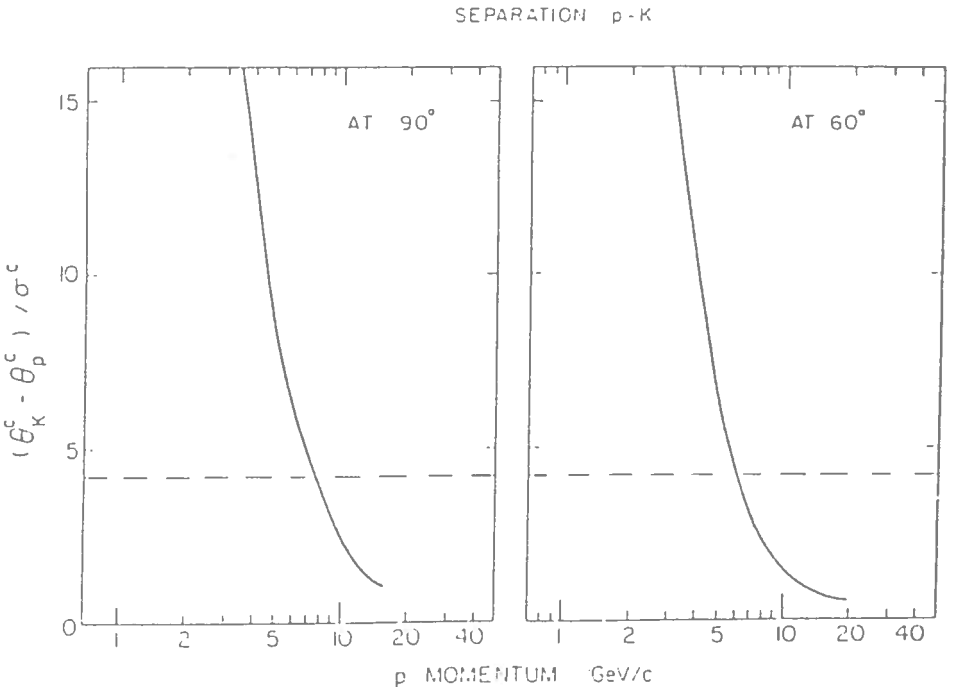

Fig.2 Estimated DELPHI π/K and K/p separation with liquid radiator.

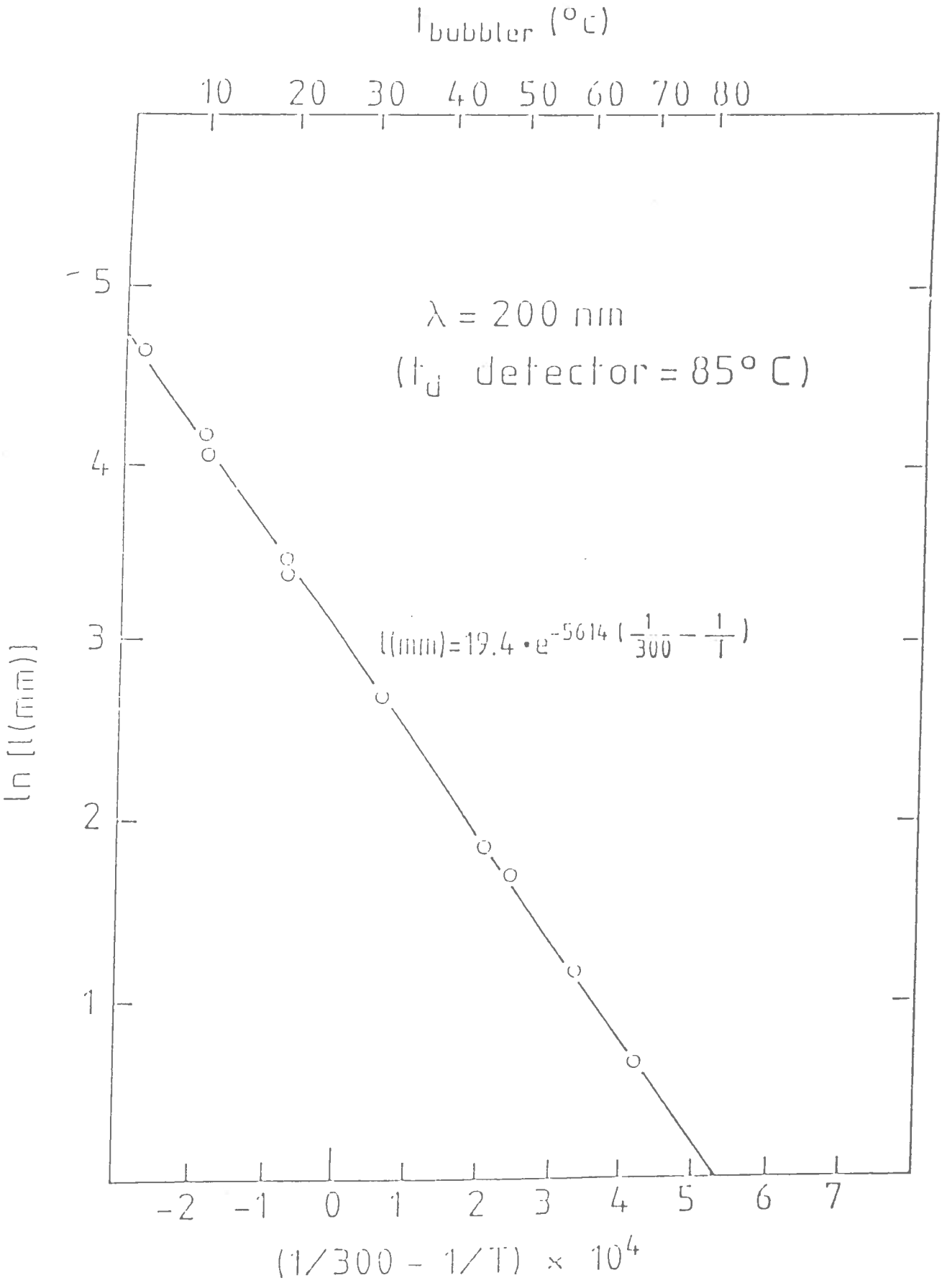

Fig.3 Photoconversion path in TMAE versus TMAE temperature (J.Seguinot private comunication).

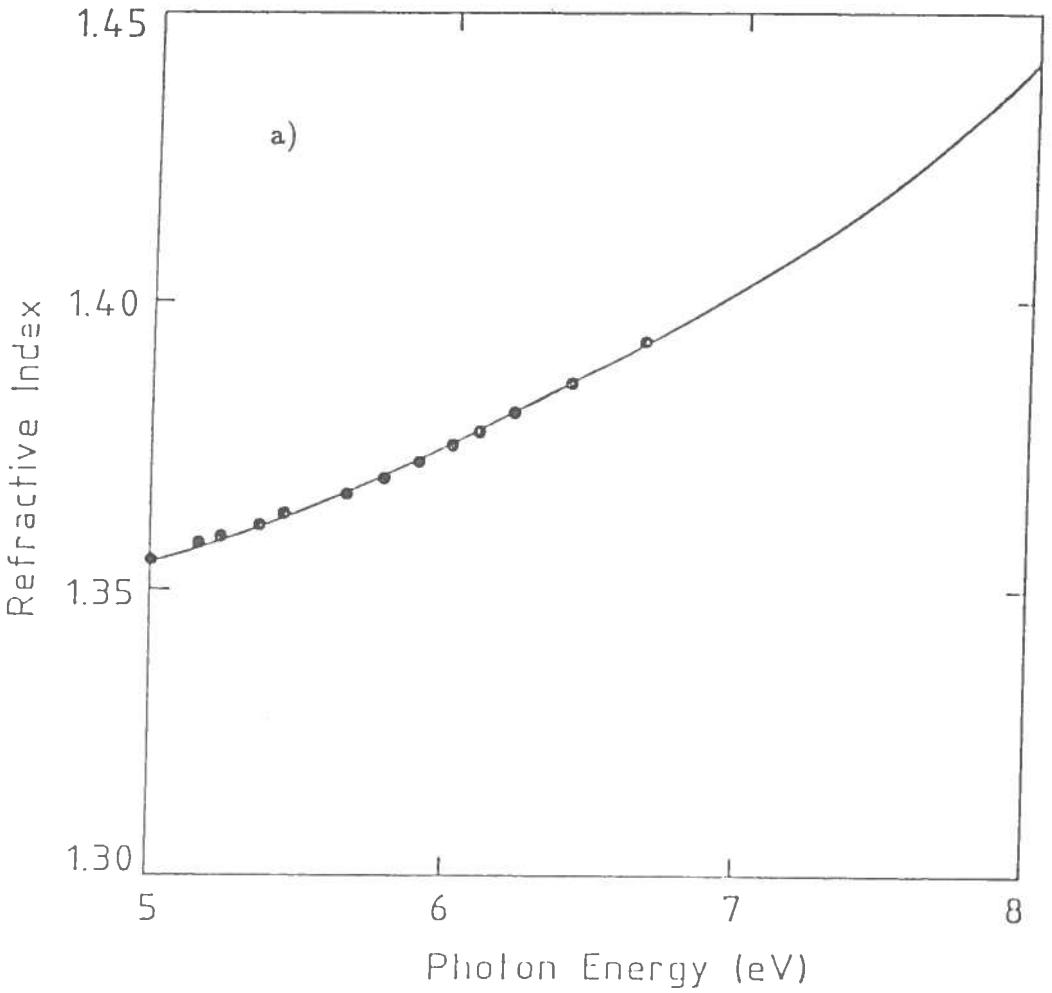

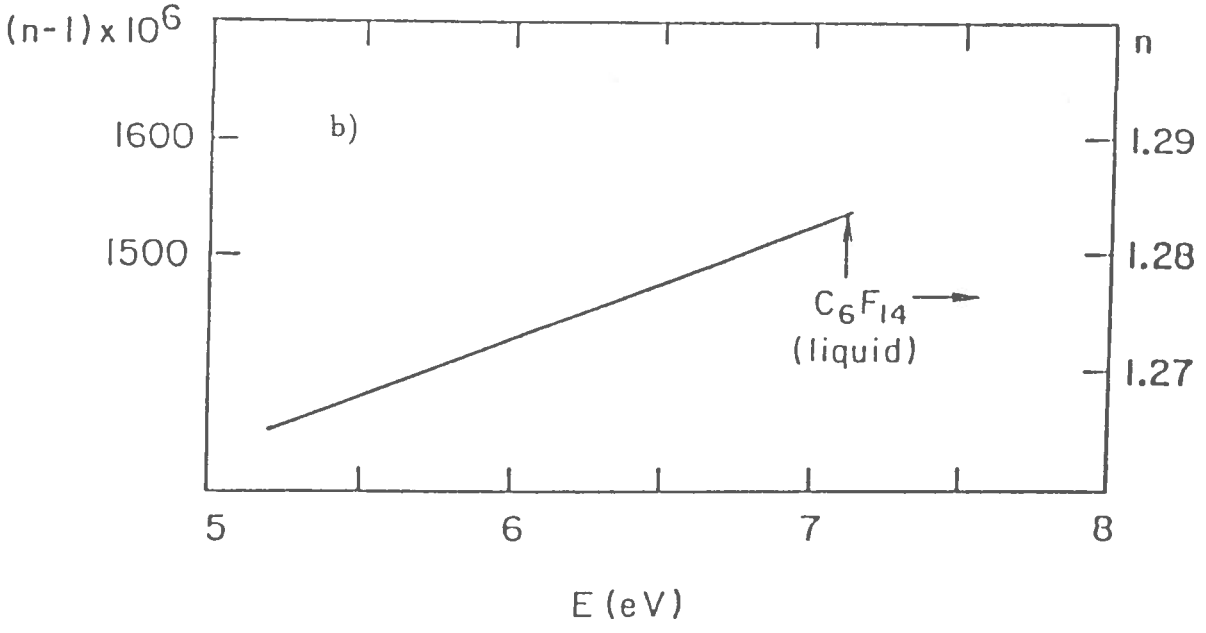

Fig.4 Refractive index n of NaF (from ref.[7]) and C_6F_{14} (from ref.[6]) versus the photon energy.

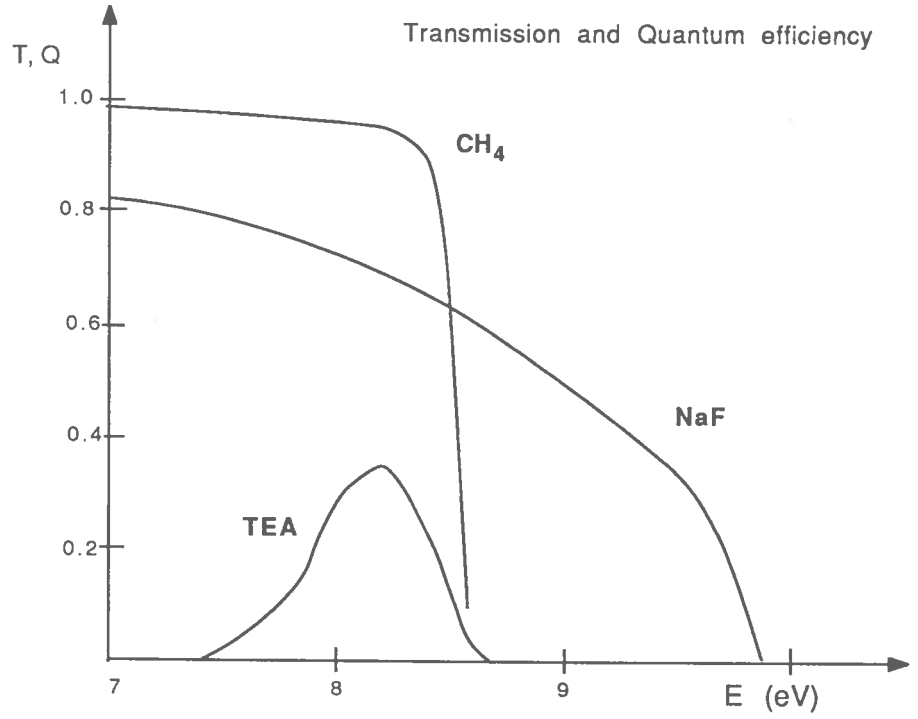

Fig.5 NaF trasmission (from ref.[7]) and TEA quantum efficiency with CH_4 cut-off (from ref.[11]) versus the photon energy.

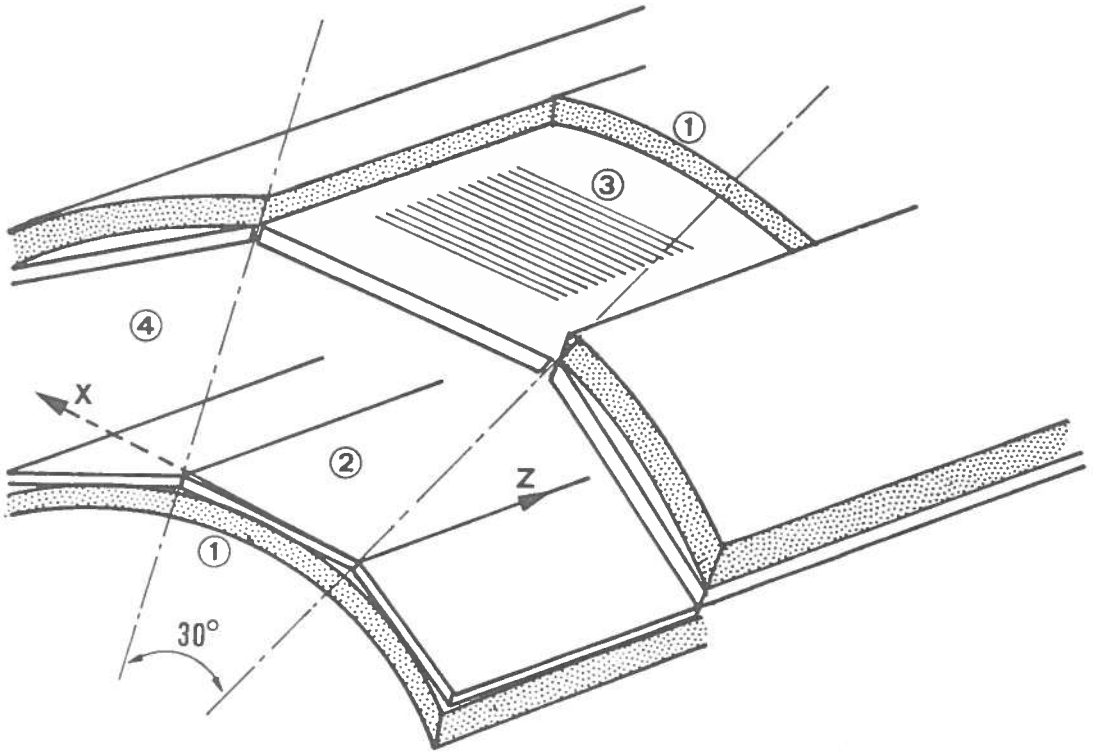

① Honeycomb vessel
② NaF radiator
③ Detector
④ He filled region

Fig.6 Schematic view of the detector.

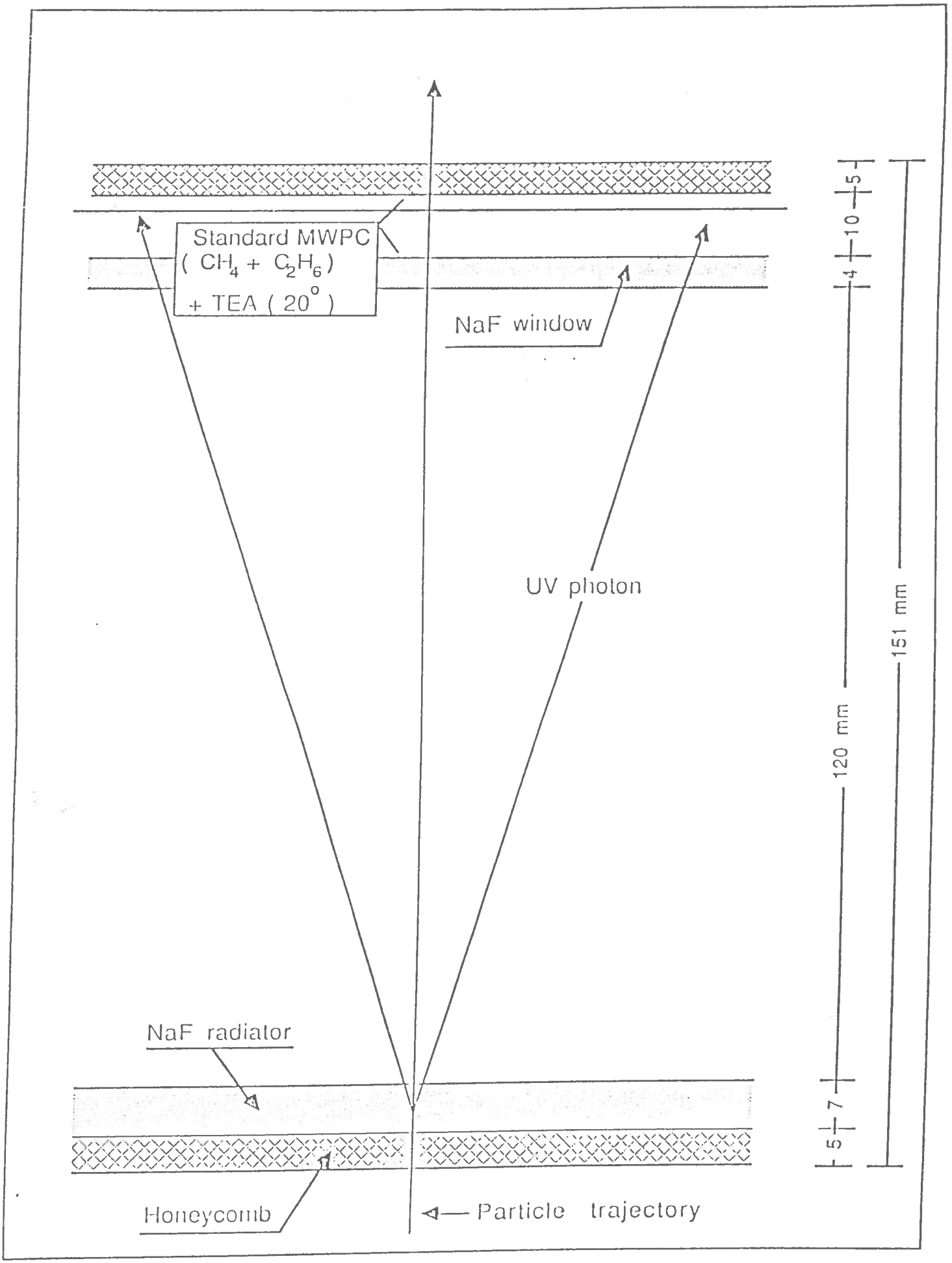

Fig.7 Sector cross section.

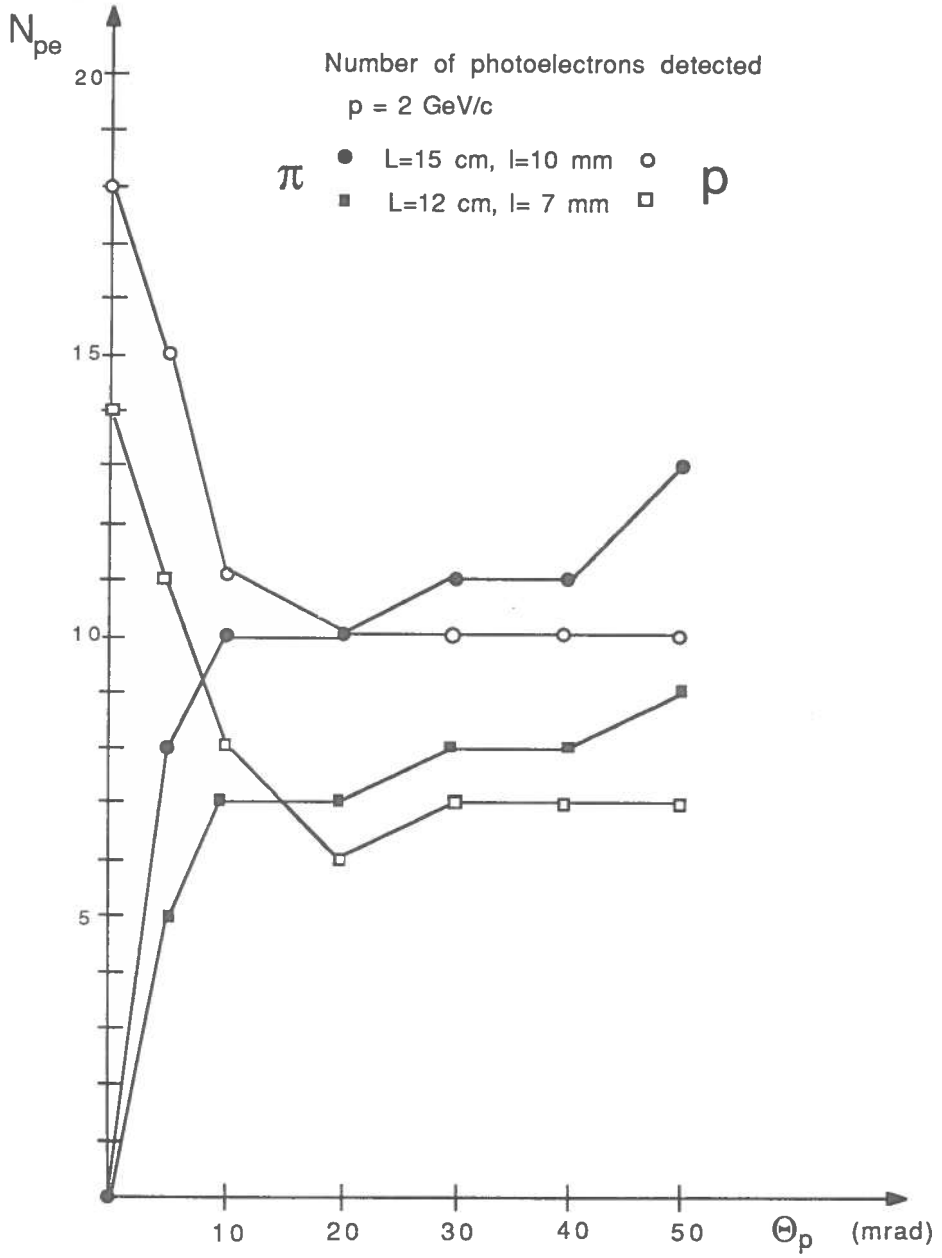

Fig.8 Number of detected photoelectrons versus the incidence angle of 2 GeV/c momentum π and p for L = 15 cm, l = 1 cm and L = 15 cm, l= 0.7 cm.

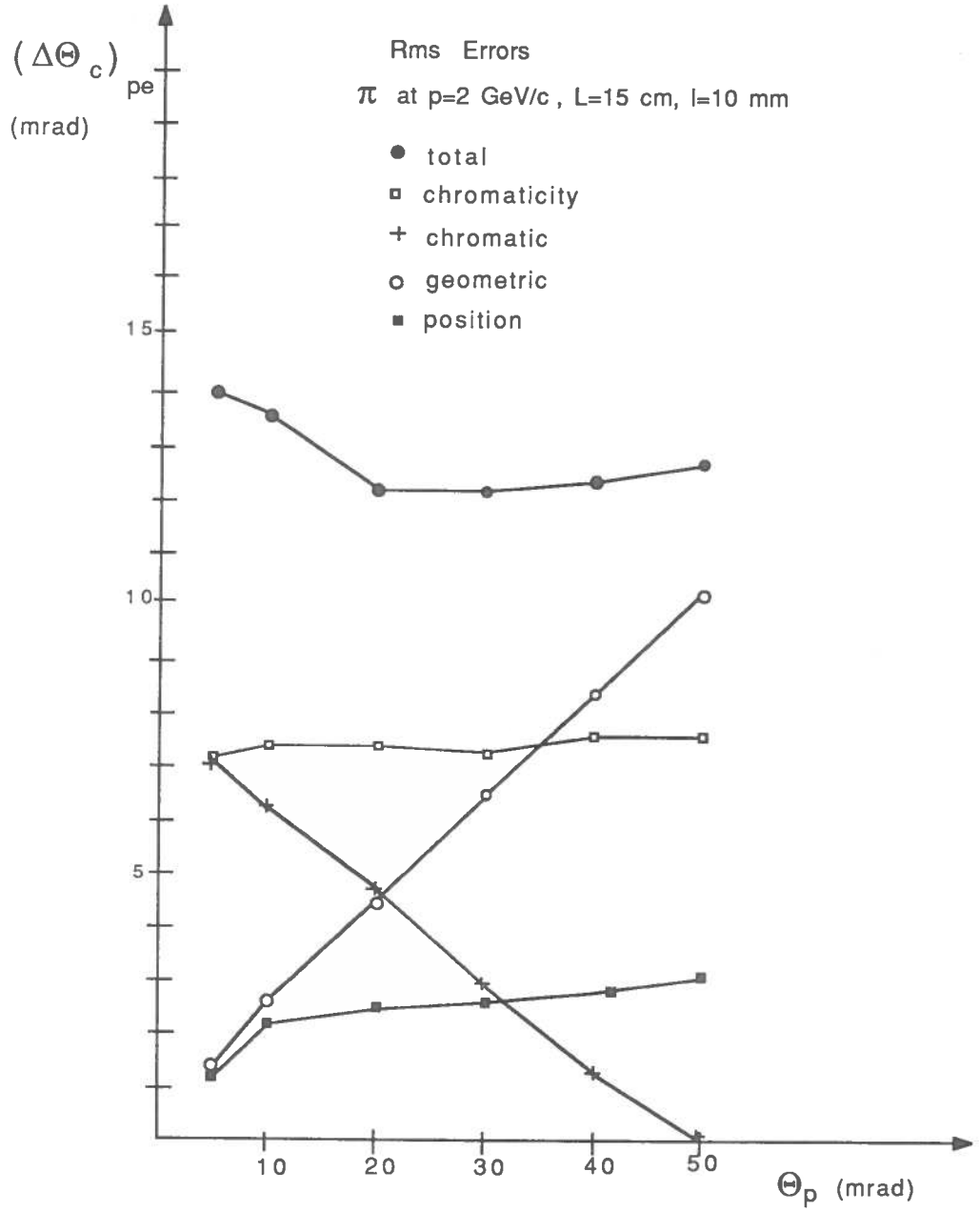

Fig.9 a Total $\Delta\theta_C$ for a 2 GeV/c momentum π versus the incidence angle with the contributions from cromaticity and chromatic, geometric and position error for L = 15 cm and l = 1 cm

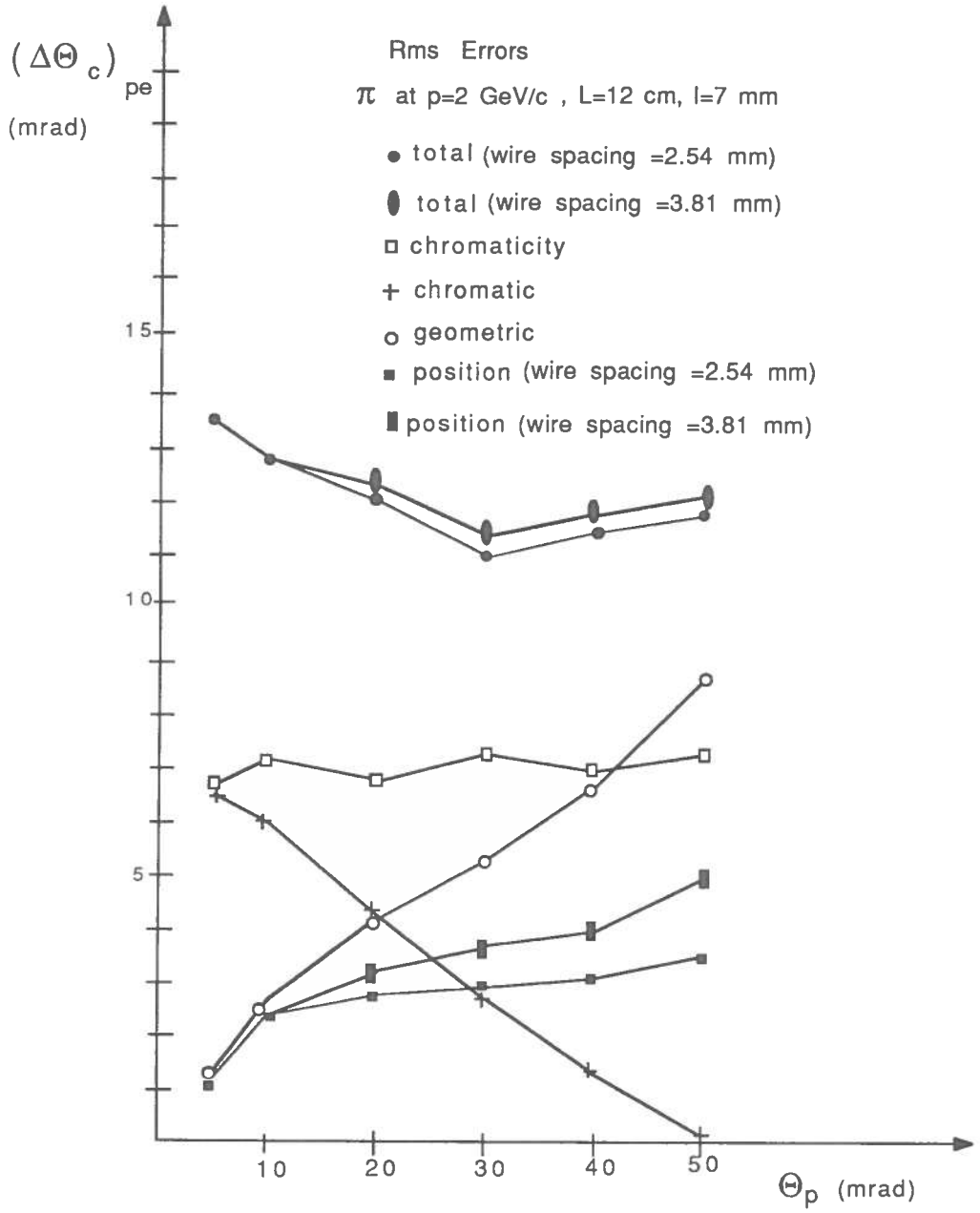

Fig.9 b Total $\Delta\theta_C$ for a 2 GeV/c momentum π versus the incidence angle with the contributions from cromaticity and chromatic, geometric and position error for L = 12 cm and l = 0.7 cm

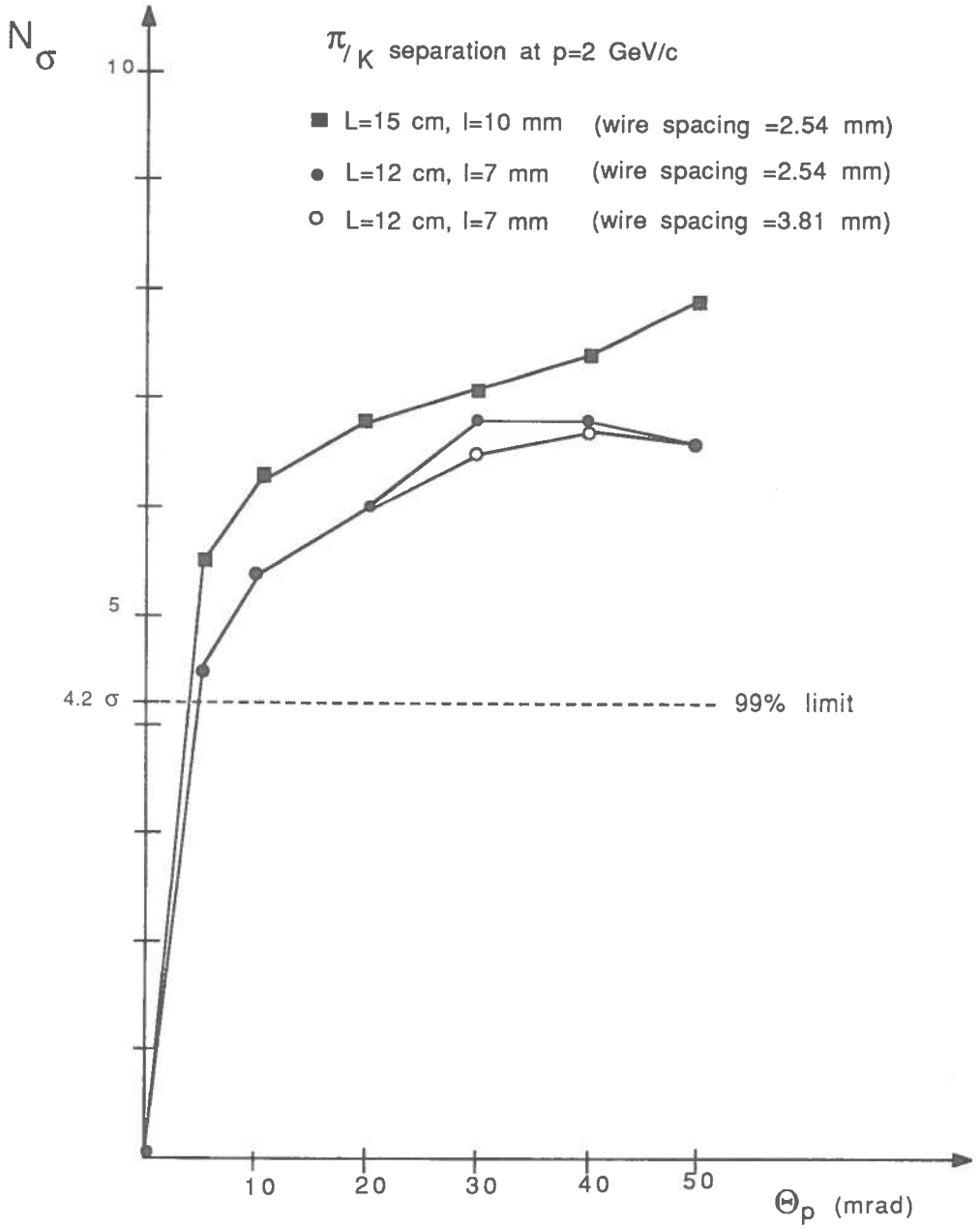

Fig.10 a π/K separation versus the incidence angle for a 2 GeV/c momentum particle for L = 15 cm, l = 1 cm and σ_z = 2.54 mm, L = 12 cm l = 0.7 cm and σ_z = 2.54 mm and for L = 12 cm, l = 0.7 cm and σ_z = 3.81 mm

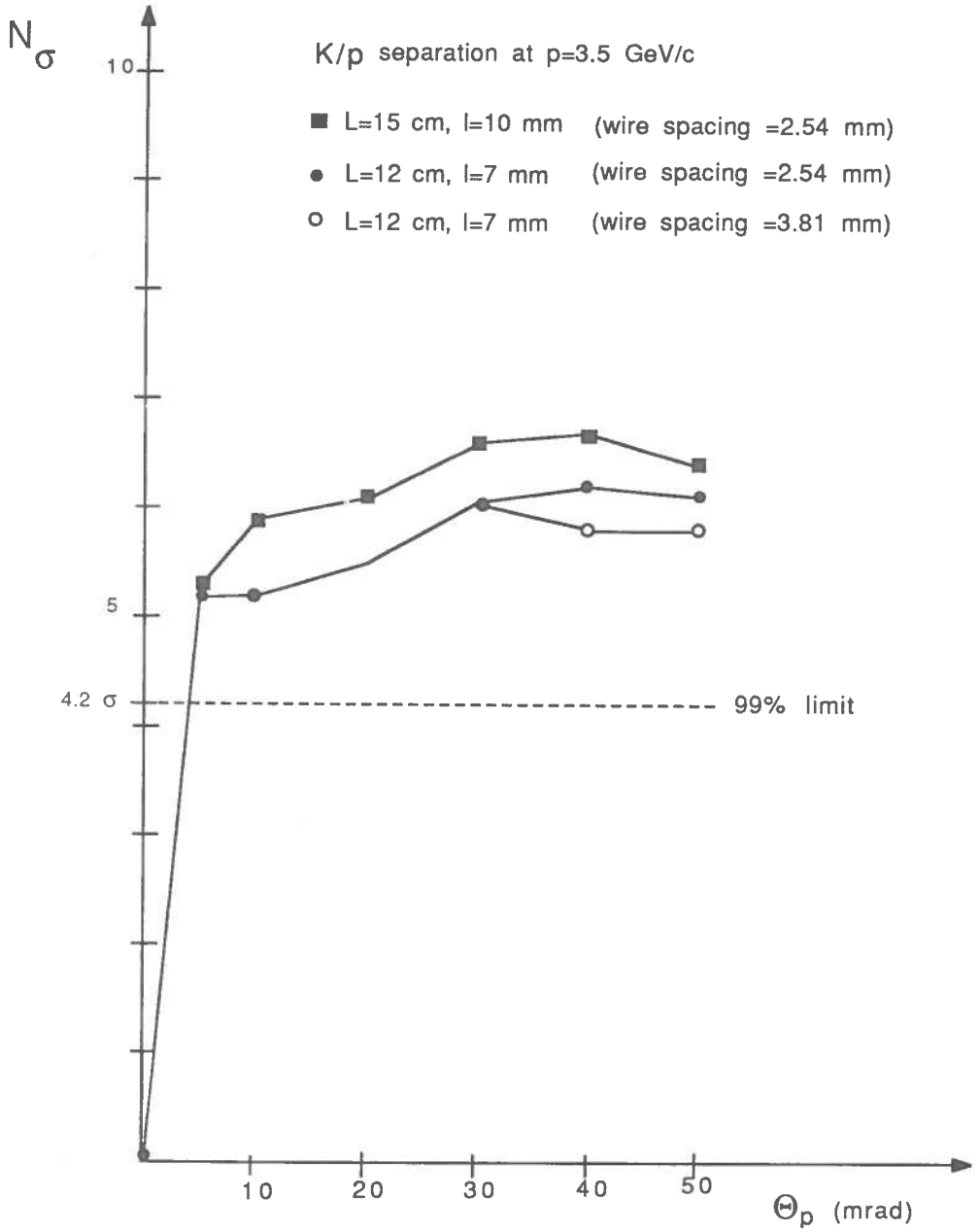

Fig.10 b K/p separation versus the incidence angle for a 2 GeV/c momentum particle for L = 15 cm, l = 1 cm and σ_z = 2.54 mm, L = 12 cm l = 0.7 cm and σ_z = 2.54 mm and for L = 12 cm, l = 0.7 cm and σ_z = 3.81 mm

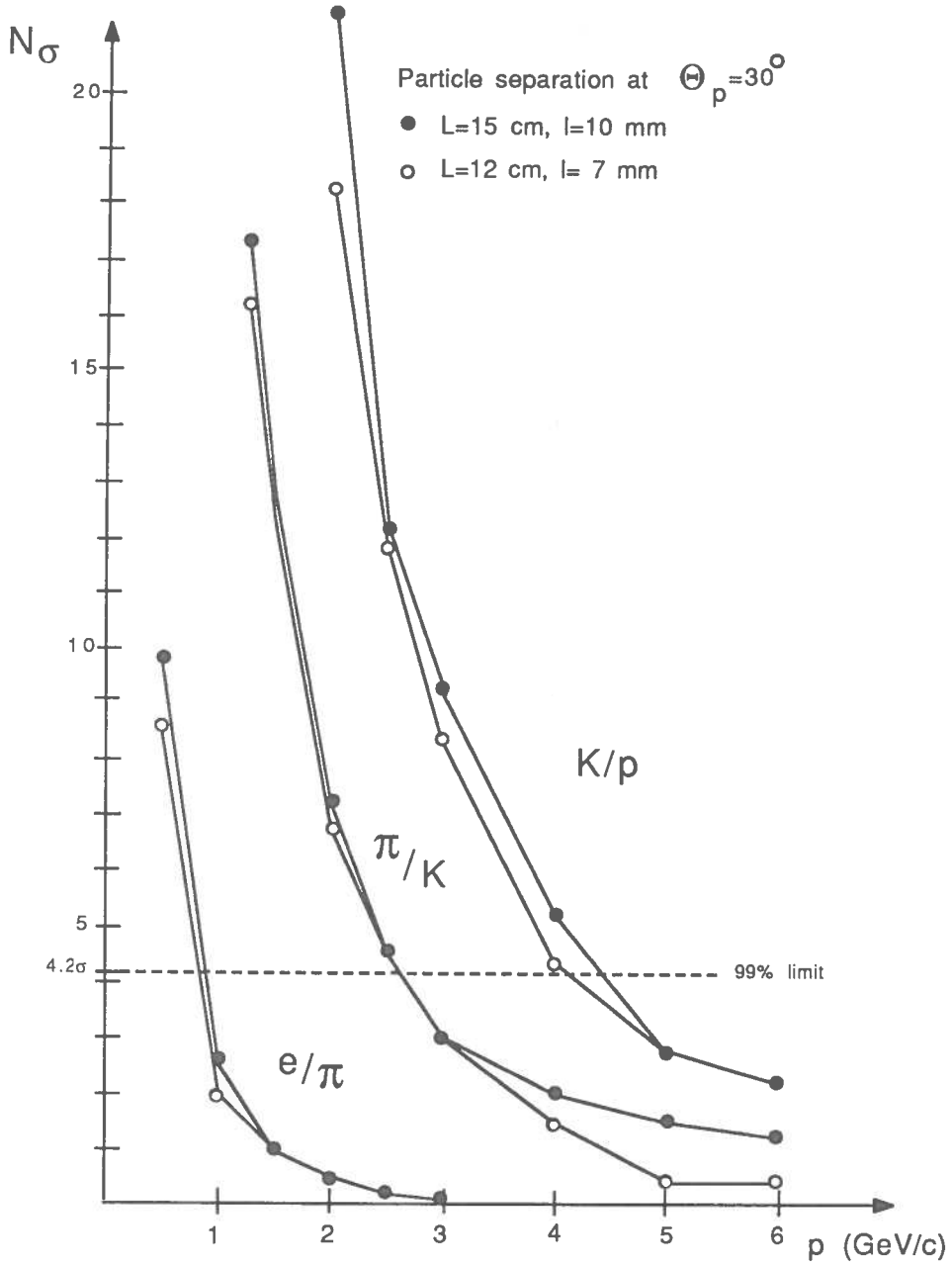

Fig.11 Particle separation at $\theta_p = 30^0$ versus the particle momentum in GeV/c, for L = 15 cm, l = 1 cm and L = 12 cm, l = 0.7 cm. Data refer to $\sigma_z = 2.54$ mm; no differencies are obtained for $\sigma_z = 3.81$ mm.

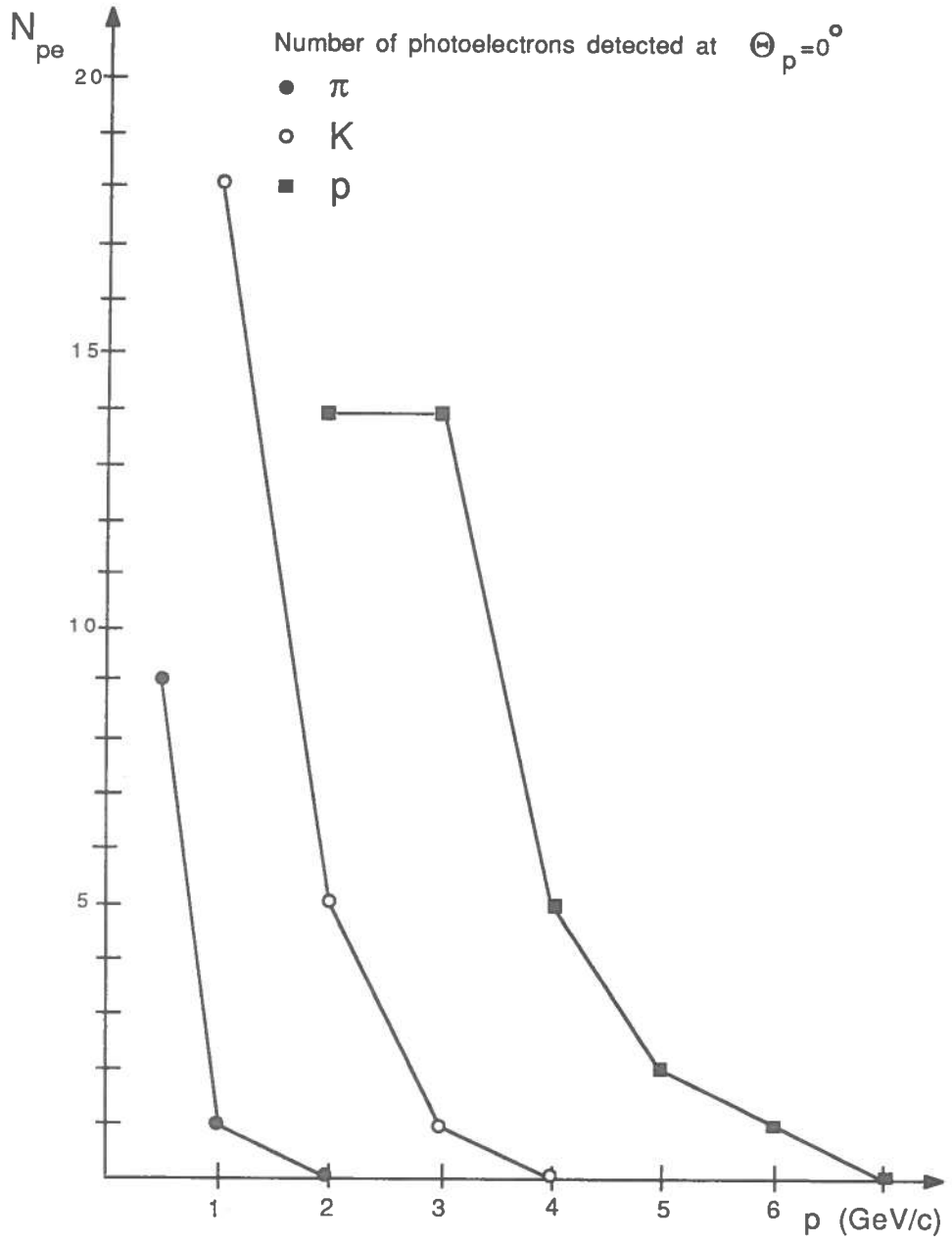

Fig.12 Number of photoelectrons detected at $\theta_p = 0^0$.

Table 1 Momentum mean values and mean multiplicities of $B\bar{B}$ events at the Y(4s).

$< E_\gamma >$	200 MeV/c^2
$< p_\pi >$	420 MeV/c
$< p_K >$	600 MeV/c
$< p_p >$	550 MeV/c
charged multiplicity	12
photon multiplicity	12

Table 2 Particle identification performances of ARGUS and CLEO II (from ref. [3]).

detector	CLEO II	ARGUS
resolution on dE/dx	6%	5%
resolution on TOF	200 *psec*	220 *psec*
3σ π/K separation up to	800 MeV/c	700 MeV/c
3σ K/p separation up to	1500 MeV/c	1200 MeV/c